Dynamics of a Duffing nanomechanical resonator coupled to a single-electron transistor: A master equation approach

Subramanian Ramakrishnan, Yuriy Gulak, and Haym Benaroya*
Department of Mechanical and Aerospace Engineering, Rutgers University, Piscataway, New Jersey 08854, USA
(Received 11 December 2007; published 11 November 2008)

We investigate the nonlinear dynamics of a classical Duffing nanomechanical resonator coupled to a single-electron transistor (SET) using a master equation formalism. We consider both the cases of hardening and softening stiffnesses of the Duffing regime while assuming linear coupling between the SET and the resonator. We first derive scaled master equations for the coupled system and define a parameter that characterizes the effective nonlinearity in the system. Solving the equations using a method of moment approximations and validating the approximations independently using finite element solutions, we conclude that the coupled system reaches a steady state and that interaction with the SET damps the motion of the resonator at a significantly higher rate in the hardening Duffing case in comparison with the case of a linear harmonic resonator. The concomitant conclusion that the steady state is attained more rapidly suggests that the hardening stiffness Duffing regime has better prospects for sensing applications than the linear regime. Moreover, analysis of the variance of the resonator displacement in the steady state indicates that lower steady-state effective temperatures are obtained in the nonlinear case. In the case of softening stiffness, dynamical instability occurs in certain parameter regimes implying that the SET transfers energy to the resonator in these regimes. Interestingly, the onset of instability is preceded by the appearance of periodic orbits in phase space. Since weak coupling between the SET and the resonator is assumed throughout, our analysis indicates that a variety of important phenomena, including negative damping, can arise from purely nonlinear motion of the nanomechanical resonator in this regime.

DOI: 10.1103/PhysRevB.78.174304 PACS number(s): 85.85.+j, 05.45.−a, 72.70.+m, 73.23.−b

I. INTRODUCTION

A nanoelectromechanical system (NEMS) may be broadly understood as a nanostructured device in which there exists significant mutual interaction between charge transport in the device and its mechanical degrees of freedom.[1–7] This electromechanical coupling implies that the current characteristics of the device may be used to study its motion characteristics. NEMS has been extensively studied in recent times due to their immense potential for such applications as ultrasensitive motion detection,[8–12] mass detection,[13,14] charge sensing,[15] and force microscopy.[16] Furthermore, they have opened up exciting avenues in fundamental research as testbeds for the direct observation of quantum behavior in mesoscopic systems, the study of quantum control and quantum computation.[17–21]

In this paper, we focus on a realization of NEMS that comprises a nanoscale to microscale high-frequency mechanical oscillator capacitively coupled to a single-electron transistor (SET). The SET operates under the principle of single-electron tunneling[22] and the key idea here is that due to the coupling, the oscillator motion leaves its signature on the SET current which can be amplified and detected for sensing applications. This system and its variants involving a superconducting single-electron transistor (SSET) have been the subject of intense experimental and theoretical research and are well recognized as an important example of NEMS.[10,19,23–26]

Given the typical high frequencies of nanoresonators (a few hundred megahertz to gigahertz), their small sizes (a few microns in each dimension), and the complex dynamical interplay between the electronic and mechanical degrees of freedom, nonlinear phenomena play an important role in NEMS dynamics. In fact, experimental evidence suggests that nonlinear effects in nanoresonators could be advantageously harnessed in applications such as signal amplification.[27–31] On the other hand, the nonlinear regime of nanoresonators is of great theoretical interest due to the occurrence of phenomena such as the transition to chaos,[32] stochastic resonance,[31] and quantum effects.[33]

Analytical models for a nanomechanical resonator coupled to a SET that account for the interaction between the device and the resonator have only relatively recently emerged in the literature. In our study of nonlinear resonator motion, we are motivated by the formalism proposed by Armour *et al.*[23] for the case of a normal-state SET weakly coupled to a resonator where the latter is modeled as a linear harmonic oscillator. We note that the Armour-Blencowe-Zhang[23] approach has been extended to the case of a SSET (Ref. 24) and the main conclusions have been verified experimentally (see, for instance, Ref. 19). Also, their model has motivated the treatment of the case of strong coupling between the SET and the resonator.[34]

In this paper, we consider the dynamics of the SET-nanoresonator system in the Duffing regime under the assumption of weak linear coupling between the device and the resonator. The assumption of linear coupling which translates to a linear variation in gate capacitance of the SET with respect to the resonator displacement is currently accepted as a reasonable one.[23] However, it is to be noted that the current state of understanding of nonlinear processes in devices such as the SET is far from complete and future work could lead to a more general treatment based on a fully nonlinear coupling between the SET and the resonator. Characteristic of

the Duffing potential is a term that is quartic in the oscillator displacement.[35] Depending on this term being added to or subtracted from the harmonic-oscillator potential, one obtains the cases of hardening and softening spring stiffnesses, respectively. Indeed, the two cases engender qualitatively different dynamics.

We first derive the master equations that govern the model in a generic way that is applicable to both the cases. Upon appropriately scaling the equations, we define a parameter that characterizes the type and strength of the effective nonlinearity in the resonator motion. We study nonlinear effects based on this parameter. We then solve the master equations using an approximate moment evolution method (MEM), validating our approximations using solutions generated independently by a finite element method (FEM). Having obtained the solutions, we then study the characteristics of the resonator motion in the Duffing regime. Primarily we are interested in whether the resonator motion is damped due to the interaction with the SET resulting in the coupled system reaching a steady state. In particular, if the damping mechanism exists, we seek to understand the differences, if any, between resonator damping in the linear and nonlinear cases. Also, if the system reaches a steady state, we are interested in the implications of the nonlinearity for the effective steady-state temperature. Finally, we address the question of the onset of dynamical instabilities associated with nonlinear motion.

The paper is organized as follows. In Sec. II we briefly discuss the system and the model whose generalization to the Duffing regime will be studied in the subsequent sections. The discussion here closely follows[23] with an emphasis on the two-nondimensional parameters κ and ϵ that play a central role in the dynamics. In Sec. III, we derive the master equations for the Duffing case and introduce a parameter η that characterizes the type and strength of the nonlinearity. In Sec. IV we derive a system of moment equations from the master equations. Infinite moment hierarchy being a generic feature of nonlinear systems, we obtain moment closure by introducing a set of approximations. The validity of the approximations is established on a case by case basis in the subsequent sections based on independently solving the master equations using a finite element method. In Sec. V we solve the moment equations for the case of the Duffing potential with hardening stiffness for different values of η and observe that the system reaches a steady state in all the cases. However, the steady state is reached much more rapidly as the strength of the nonlinearity is increased. In other words, the damping rate increases remarkably with increasing values of η. Furthermore, the variance of the displacement in the steady state decreases with increasing η. In Sec. VI we solve the case of the Duffing potential with softening stiffness and observe that the SET back action is less efficient in damping the resonator motion than the linear case even in the presence of very weak nonlinearity. As the magnitude of η is increased, the SET back action becomes increasingly incapable of damping the resonator motion. Eventually a critical value of η is reached at which the SET and the resonator exist in equilibrium where we observe a periodic orbit in the phase space of the resonator. Beyond this critical value of η, we observe the onset of instability. We conclude the paper in Sec. VII with a discussion of our results and their implications for sensing applications of the SET-nanoresonator system.

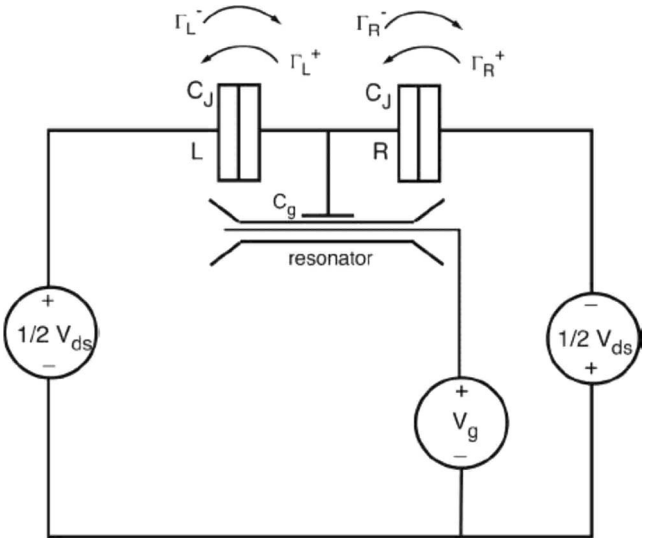

FIG. 1. Circuit diagram of a SET-resonator system.

II. SET-RESONATOR SYSTEM AND THE ANALYTICAL MODEL

A. SET-resonator system

A schematic of the system studied in this paper is presented in Fig. 1, reproduced from Ref. 7. The SET comprises of the left and right tunnel junctions (indicated by L and R in the figure) as well as the gate (island) whose capacitance is labeled C_g in the figure. The gate voltage is denoted by V_g and the drain-source voltage by $V_{\rm ds}$. The tunneling rates across the left and right junctions are given by $\Gamma_{L/R}^{\pm}$ where the plus and minus signs indicate the direction of tunneling.

B. Analytical model

In this section we discuss the analytical model for the SET-resonator system proposed by Armour *et al.*[23] The starting point is the orthodox model for a stand-alone SET.[22] The only two accessible dynamical states of the SET considered are those with N or $N+1$ electrons in the central island and the orthodox model characterizes these mutually exclusive states by probabilities $p_N(t)$ and $p_{N+1}(t)$ that correspond to the probabilities of finding N or $N+1$ electrons in the island at time t, respectively. The time evolutions of these probabilities are governed by a pair of coupled master equations given by[22]

$$\frac{dp_N}{dt} = -(\Gamma_L^- + \Gamma_R^+)p_N + (\Gamma_L^+ + \Gamma_R^-)p_{N+1}, \tag{1}$$

$$\frac{dp_{N+1}}{dt} = (\Gamma_L^- + \Gamma_R^+)p_N - (\Gamma_L^+ + \Gamma_R^-)p_{N+1}, \tag{2}$$

where $\Gamma_{L/R}^{\pm}$ represent the tunneling rates in the left (L) and right (R) junctions of the SET island. Here the $\pm$ signs indi-

cate that tunneling, under very general conditions, is possible in both directions. The expressions for the tunneling rates are given by Fermi's golden rule and take the final form,[22,36]

$$\Gamma_{L/R}^{\pm} = \frac{1}{e^2 R_J} \frac{E_{L/R}^{\pm}}{[1 - \exp(-E_{L/R}^{\pm}/k_B T_e)]}. \quad (3)$$

In the above expression e represents the electron charge, R_J the effective junction resistance (assumed identical for both junctions of the island), k_B the Boltzmann constant, T_e the temperature of the source, drain, and island electron reservoirs (all assumed equal), and $E_{L/R}^{\pm}$ the energy gained by a single-electron tunneling to the left (+) or to the right (−) across the left (L) or right (R) junction.

The significant step taken in Ref. 23 is the modification of the above master equations to incorporate the dynamics of the resonator. The state of the resonator can be described by a continuous probability density function $P(x,u;t)$ where x stands for the position and u stands for the velocity of the resonator. Now, since for each state of the resonator the SET can be in either of the states N or $N+1$, one needs to be able to define the probability of finding the SET in either of these states, given that the probability density of the resonator is $P(x,u;t)$. To this end, the model defines a decomposition of P into $P(x,u;t)=P_N(x,u;t)+P_{N+1}(x,u;t)$ where the functions P_N and P_{N+1} are called subdensities and are used to define the probabilities of the finding the SET in the N or $N+1$ states, respectively, given that the resonator is in the state (x,u) at time t.

Since the transition of the SET island from the N electron state to the $N+1$ electron state (and vice versa) is guaranteed to alter the dynamical state of the resonator, the resonator Hamiltonian corresponding to the two states is denoted by H_N and H_{N+1}. The key idea now is to treat the probability subdensities P_N and P_{N+1} as dynamical variables evolving under the corresponding Hamiltonians H_N and H_{N+1}. At once, Liouville's theorem can be invoked to incorporate the resonator dynamics into the orthodox model master equations [Eqs. (1) and (2)] to write the generalized master equations for the SET-nanoresonator system as

$$\frac{\partial P_N}{\partial t} = \{H_N, P_N\} - (\Gamma_L^- + \Gamma_R^+)P_N + (\Gamma_L^+ + \Gamma_R^-)P_{N+1}, \quad (4)$$

$$\frac{\partial P_{N+1}}{\partial t} = \{H_{N+1}, P_N\} + (\Gamma_L^- + \Gamma_R^+)P_N - (\Gamma_L^+ + \Gamma_R^-)P_{N+1}. \quad (5)$$

The next crucial step in order to achieve coupling between the resonator motion and the tunneling process is to calculate the tunneling rates in terms of H_N and H_{N+1}. We refer to Ref. 23 for the details of this calculation and the assumptions involved therein. The master equations are obtained in explicit form as

$$\frac{\partial P_N}{\partial t} = \omega_0^2(x)\frac{\partial P_N}{\partial u} - u\frac{\partial P_N}{\partial x} + \frac{1}{e^2 R_J}[E_L P_{N+1} - E_R P_N - m\omega_0^2 x_0 x P], \quad (6)$$

$$\frac{\partial P_{N+1}}{\partial t} = \omega_0^2(x - x_0)\frac{\partial P_{N+1}}{\partial u} - u\frac{\partial P_{N+1}}{\partial x} - \frac{1}{e^2 R_J}[E_L P_{N+1} - E_R P_N - m\omega_0^2 x_0 x P], \quad (7)$$

where the left and the right tunneling rates are now given by

$$E_L = -2E_c N' - m\omega_0^2 x_0^2 (N_g - N' - 1/2) + eV_{ds}/2, \quad (8)$$

$$E_R = 2E_c N' + m\omega_0^2 x_0^2 (N_g - N' - 1/2) + eV_{ds}/2. \quad (9)$$

In the above expressions for E_L and E_R, $E_c = e^2/2C$ is the island charging energy where e is the electron charge and C is the total SET capacitance. $N' = N_g - N - 1/2$ is a constant defined to simplify the algebra. In the definition of N', the quantity N_g is called the charge induced by the gate voltage and is defined by $N_g = C_g V_g / e$ where C_g and V_g are the gate capacitance and the gate voltage, respectively. Also, m is the mass of the resonator, ω_0 is the natural frequency of oscillation, and x_0 is the shift in resonator position induced by a tunneling electron and is explicitly defined as $x_0 = -e^2 N_g / Cm\omega_0^2 d$, where d is the resonator-SET island gap.

We note here that, applying the scaling transforms $u' = u/u_0$, $x' = x/x_0$, and $t' = t/\tau_t$ where τ_t is the electron-tunneling time that defines the characteristic time scale of processes in the SET, x_0 is the characteristic displacement of the resonator, and $u_0 = x_0/\tau_t$, the master equations may be written in nondimensional form as[7]

$$\frac{\partial P_N}{\partial t} = \epsilon^2 x\frac{\partial P_N}{\partial u} - u\frac{\partial P_N}{\partial x} + \tilde{E}_L P_{N+1} - \tilde{E}_R P_N, \quad (10)$$

$$\frac{\partial P_{N+1}}{\partial t} = \epsilon^2 (x - 1)\frac{\partial P_{N+1}}{\partial u} - u\frac{\partial P_{N+1}}{\partial x} - \tilde{E}_L P_{N+1} + \tilde{E}_R P_N, \quad (11)$$

where the dimensionless parameters ϵ and κ are introduced. The parameter ϵ, defined as $\epsilon = \omega_0 \tau_t$, characterizes the separation between the resonator and SET dynamical time scales. We again note that τ_t, the time taken by an electron to tunnel onto or off of the island, defines the characteristic time scale of the SET. The other dimensionless parameter is defined as $\kappa = m\omega_0^2 x_0^2 / eV_{ds}$ and characterizes the coupling strength between the resonator and the SET. The dimensionless energy terms $\tilde{E}_L$ and $\tilde{E}_R$ can be expressed as[23]

$$\tilde{E}_L = -\frac{e}{CV_{ds}}\left(N_g - N - \frac{1}{2}\right) - \kappa N + \frac{1}{2} - \kappa x, \quad (12)$$

$$\tilde{E}_R = +\frac{e}{CV_{ds}}\left(N_g - N - \frac{1}{2}\right) + \kappa N + \frac{1}{2} + \kappa x. \quad (13)$$

In the model, the parameters κ and ϵ hold the key to describing the coupled SET-resonator dynamics. In general, the electron-tunneling time is much smaller compared to the oscillator period and hence practical situations are best described by small values for ϵ. Likewise, strong interaction between the SET and the resonator complicates the dynamics to the extent that the model loses its validity. Hence it is

important to consider small values for κ as well.

III. MASTER EQUATIONS FOR THE DUFFING RESONATOR

In our analysis of the Duffing resonator motion we assume that the island charging energy E_c of the SET is large in comparison with the electronic thermal energy $k_B T_e$ and the drain-source bias eV_{ds}. We do not consider external damping effects. Moreover, since little is currently known about nonlinear behavior of the SET, we neglect the nonlinear terms in the Hamiltonian in calculating the tunneling rates in the device. In other words, in our approach the nonlinear effects are confined to the resonator motion via the Poisson bracket terms in the master equations derived in Ref. 23. This important assumption is further buttressed by the fact that in all the current models of the SET-resonator system, the gate capacitance of the SET is assumed to be a linear function of the oscillator displacement. This is tantamount to our approach of considering only the linear terms of the Hamiltonian in calculating the SET tunneling rate.

Consider a Duffing nanoresonator with resonator Hamiltonians for the N and $N+1$ states of the system given by

$$H_N = \frac{p^2}{2m} + \frac{1}{2}m\omega_0^2[x^2 + \beta x^4], \tag{14}$$

$$H_{N+1} = \frac{p^2}{2m} + \frac{1}{2}m\omega_0^2[(x-x_0)^2 + \beta(x-x_0)^4]. \tag{15}$$

Here p represents the momentum, m the mass, and ω_0 the frequency of the resonator. The quantity x_0 is the distance between the equilibrium positions of the resonator corresponding to the N and $N+1$ states of the SET island. In comparison with a linear harmonic oscillator, the difference is the added term βx^4 in the potential energy. This is the generic potential for a Duffing system and β is a constant, the magnitude of which determines the strength of the quartic order term in the potential function. The sign of β determines the geometry of the potential function and the two cases of β being positive or negative engender qualitatively different dynamics.

Computing the Poisson brackets of the resonator Hamiltonians H_N and H_{N+1} with P_N and P_{N+1}, retaining the tunneling terms from Eqs. (6) and (7), and defining the constant $\alpha = 2\beta$, we can write the master equations for the Duffing case as

$$\frac{\partial P_N}{\partial t} = \omega_0^2(x + \alpha x^3)\frac{\partial P_N}{\partial u} - u\frac{\partial P_N}{\partial x} + \frac{1}{e^2 R}[E_L P_{N+1} - E_R P_N - m\omega_0^2 x_0 x P], \tag{16}$$

$$\frac{\partial P_{N+1}}{\partial t} = \omega_0^2[(x-x_0) + \alpha(x-x_0)^3]\frac{\partial P_{N+1}}{\partial u} - u\frac{\partial P_{N+1}}{\partial x} - \frac{1}{e^2 R}[E_L P_{N+1} - E_R P_N - m\omega_0^2 x_0 x P]. \tag{17}$$

Applying the scaling transforms $u' = u/u_0$, $x' = x/x_0$, and $t' = t/\tau_t$ to Eqs. (16) and (17) where τ_t is the electron-tunneling time that defines the characteristic time scale of processes in the SET, x_0 is the characteristic displacement of the resonator as defined in Sec. II, $u_0 = x_0/\tau_t$, and recalling the definitions of ϵ and κ from Sec. II, we can write the nondimensional form of the master equations as

$$\frac{\partial P_N}{\partial t} = \epsilon^2[x + \alpha x_0^2 x^3]\frac{\partial P_N}{\partial u} - u\frac{\partial P_N}{\partial x} + \left[\frac{P_{N+1}}{2} - \frac{P_N}{2} - \kappa x P\right], \tag{18}$$

$$\frac{\partial P_{N+1}}{\partial t} = \epsilon^2[(x-1) + \alpha x_0^2(x-1)^3]\frac{\partial P_{N+1}}{\partial u} - u\frac{\partial P_{N+1}}{\partial x} - \left[\frac{P_{N+1}}{2} - \frac{P_N}{2} - \kappa x P\right]. \tag{19}$$

Parameter η

Comparing Eqs. (18) and (19) with the master equations in the case of a linear resonator [Eqs. (6) and (7)], it is evident that nonlinearity in the resonator contributes the terms $\alpha x_0^2 x^3$ and $\alpha x_0^2(x-1)^3$ to the master equations. The only other parameters in the equations are κ and ϵ. Hence we define

$$\eta = \alpha x_0^2. \tag{20}$$

We make the following observations about η. First, since x_0^2 is always positive, η is guaranteed to faithfully reflect sign changes in α. Therefore, changing the sign of η allows us to unambiguously represent the hardening and softening stiffness Duffing potentials. Second, η is the true index of the effective nonlinearity in the SET-resonator system. Consider a weakly nonlinear resonator that corresponds to a relatively small value of α. However, a relatively high value of x_0 [resulting from a relatively stronger coupling between the SET and the resonator since x_0 is the resonator displacement induced by the $(N+1)$th electron tunneling onto the SET island] even under this circumstance implies a higher value of η thereby amplifying the nonlinear effect. On the other hand, we have the expected conclusion that a higher value of α implies a higher η even if the coupling between the device and the resonator is weak (smaller x_0). Third, as a parameter that dictates the dynamics, η is to be treated on par with κ and ϵ. Indeed, in the sequel we discuss all uniquely nonlinear effects in terms of η. We now write the master equations in their final form as

$$\frac{\partial P_N}{\partial t} = \epsilon^2[x + \eta x^3]\frac{\partial P_N}{\partial u} - u\frac{\partial P_N}{\partial x} + \left[\frac{P_{N+1}}{2} - \frac{P_N}{2} - \kappa x P\right], \tag{21}$$

$$\frac{\partial P_{N+1}}{\partial t} = \epsilon^2[(x-1) + \eta(x-1)^3]\frac{\partial P_{N+1}}{\partial u} - u\frac{\partial P_{N+1}}{\partial x} - \left[\frac{P_{N+1}}{2} - \frac{P_N}{2} - \kappa x P\right]. \tag{22}$$

IV. MOMENT EVOLUTION EQUATIONS

A straightforward method of solving the master equations is to solve the associated system of moment evolution equations. However, in the case of nonlinear systems the moment hierarchy grows unboundedly and hence judicious approximations are imperative in obtaining solutions. In this section we derive the exact moment equations, introduce a set of approximations, and arrive at the final set of equations to be solved.

In order to set the notation we adopt standard terminology from probability theory and denote the mean value of an arbitrary random process $s(t)$ at time t with respect to the density P as

$$\langle s\rangle = \int dx \int dus P. \tag{23}$$

Similarly, the averages with respect to $P_N(x,u;t)$ and $P_{N+1}(x,u;t)$ are, respectively, defined as

$$\langle s\rangle_N = \int dx \int dus P_N,$$

$$\langle s\rangle_{N+1} = \int dx \int dus P_{N+1}. \tag{24}$$

In Eq. (24) the limits of integration for both variables x and u are defined by the open interval $(-\infty,\infty)$. We recall that by construction, $P(x,u;t)=P_N+P_{N+1}$. Carrying out straightforward calculations based on Eqs. (21) and (22) we obtain the moment evolution equations in the notation defined in Eq. (24) as

$$\frac{d\langle x\rangle}{dt} = \langle u\rangle, \tag{25}$$

$$\frac{d\langle u\rangle}{dt} = -\epsilon^2[\langle x\rangle + \eta\langle x^3\rangle] + \epsilon^2(1+\eta)\langle P\rangle_{N+1} - 3\epsilon^2\eta\langle x\rangle_{N+1} + 3\epsilon^2\eta\langle x^2\rangle_{N+1}, \tag{26}$$

$$\frac{d\langle P\rangle_{N+1}}{dt} = -\langle P\rangle_{N+1} + \frac{1}{2} + \kappa\langle x\rangle, \tag{27}$$

$$\frac{d\langle x^3\rangle}{dt} = 3\langle x^2 u\rangle, \tag{28}$$

$$\frac{d\langle x\rangle_{N+1}}{dt} = \langle u\rangle_{N+1} - \langle x\rangle_{N+1} + \frac{1}{2}\langle x\rangle + \kappa\langle x^2\rangle, \tag{29}$$

$$\frac{d\langle x^2\rangle_{N+1}}{dt} = 2\langle ux\rangle_{N+1} - \langle x^2\rangle_{N+1} + \frac{1}{2}\langle x^2\rangle + \kappa\langle x^3\rangle, \tag{30}$$

$$\frac{d\langle x^2\rangle}{dt} = 2\langle ux\rangle, \tag{31}$$

$$\frac{d\langle u\rangle_N}{dt} = -\epsilon^2[\langle x\rangle_N + \eta\langle x^3\rangle_N] + \frac{1}{2}\langle u\rangle - \kappa\langle xu\rangle + \langle u\rangle_N, \tag{32}$$

$$\frac{d\langle x^3\rangle_N}{dt} = 3\langle x^2 u\rangle_N. \tag{33}$$

That the number of equations in the above system continues to grow if we were to attempt a further decoupling of the moments of the products raises the question as to why a system of nine equations is chosen. The answer lies in the fact that the solutions obtained from the moment equation approach (at different levels of approximation) can be readily compared with our finite element solutions and we found the above system of equations to be optimal. In order to obtain closure for the above set of moment evolution equations, after exploring various possibilities, we arrived at the following decoupling approximations. As will be discussed in the sequel these approximations are justified based on the finite element solutions. It is also noted here that the approximations assume decoupling between moments of positions and velocities. Since position and velocity are independent variables in phase space, the assumptions of decoupling between their moments are more justifiable than similar assumptions between higher moments of the same variable. The approximations are

$$\langle x^2 u\rangle = \langle x^2\rangle\langle u\rangle,$$

$$\langle ux\rangle_{N+1} = \langle u\rangle_{N+1}\langle x\rangle_{N+1},$$

$$\langle ux\rangle = \langle u\rangle\langle x\rangle,$$

$$\langle x^2 u\rangle_N = \langle x^2\rangle_N\langle u\rangle_N. \tag{34}$$

Introducing the approximations [Eq. (34)] into the moment evolution equations we can write the decoupled system of equations as

$$\frac{d\langle x\rangle}{dt} = \langle u\rangle, \tag{35}$$

$$\frac{d\langle u\rangle}{dt} = -\epsilon^2[\langle x\rangle + \eta\langle x^3\rangle] + \epsilon^2(1+\eta)\langle P\rangle_{N+1} - 3\epsilon^2\eta\langle x\rangle_{N+1} + 3\epsilon^2\eta\langle x^2\rangle_{N+1}, \tag{36}$$

$$\frac{d\langle P\rangle_{N+1}}{dt} = -\langle P\rangle_{N+1} + \frac{1}{2} + \kappa\langle x\rangle, \tag{37}$$

$$\frac{d\langle x^3\rangle}{dt} = 3\langle x^2\rangle\langle u\rangle, \tag{38}$$

$$\frac{d\langle x\rangle_{N+1}}{dt} = \langle u\rangle_{N+1} - \langle x\rangle_{N+1} + \frac{1}{2}\langle x\rangle + \kappa\langle x^2\rangle, \tag{39}$$

$$\frac{d\langle x^2\rangle_{N+1}}{dt} = 2\langle u\rangle_{N+1}\langle x\rangle_{N+1} - \langle x^2\rangle_{N+1} + \frac{1}{2}\langle x^2\rangle + \kappa\langle x^3\rangle, \tag{40}$$

$$\frac{d\langle x^2\rangle}{dt} = 2\langle u\rangle\langle x\rangle, \tag{41}$$

$$\frac{d\langle u\rangle_N}{dt} = -\epsilon^2[\langle x\rangle_N + \eta\langle x^3\rangle_N] + \frac{1}{2}\langle u\rangle - \kappa\langle x\rangle\langle u\rangle + \langle u\rangle_N, \tag{42}$$

$$\frac{d\langle x^3\rangle_N}{dt} = 3\langle x^2\rangle_N\langle u\rangle_N. \tag{43}$$

We now make note of the following identities that arise from the construction $P(x,u;t)=P_N+P_{N+1}$:

$$\langle u\rangle = \langle u\rangle_N + \langle u\rangle_{N+1}, \tag{44}$$

$$\langle x^2\rangle = \langle x^2\rangle_N + \langle x^2\rangle_{N+1}. \tag{45}$$

For convenience we now label the quantities in Eqs. (35)–(43) as follows:

$$\langle x\rangle = X_1,$$

$$\langle u\rangle = X_2,$$

$$\langle P\rangle_{N+1} = X_3,$$

$$\langle x^3\rangle = X_4,$$

$$\langle x\rangle_{N+1} = X_5,$$

$$\langle x^2\rangle_{N+1} = X_6,$$

$$\langle x^2\rangle = X_7,$$

$$\langle u\rangle_N = X_8,$$

$$\langle x^3\rangle_N = X_9. \tag{46}$$

Using Eqs. (44)–(46) we write Eqs. (35)–(43) in the new variables as

$$\dot{X}_1 = X_2,$$

$$\dot{X}_2 = -\epsilon^2[X_1 + \eta X_4] + \epsilon^2(1+\eta)X_3 - 3\epsilon^2\eta X_5 + 3\epsilon^2\eta X_6,$$

$$\dot{X}_3 = -X_3 + \frac{1}{2} + \kappa X_1,$$

$$\dot{X}_4 = 3X_2X_7,$$

$$\dot{X}_5 = [X_2 - X_8]X_5 - X_5 + \frac{1}{2}X_1 + \kappa X_7,$$

$$\dot{X}_6 = 2[X_2 - X_8]X_5 - X_6 + \frac{1}{2}X_7 + \kappa X_4,$$

$$\dot{X}_7 = 2X_1X_2,$$

$$\dot{X}_8 = -\epsilon^2[X_1 - X_5 + \eta X_9] + \frac{1}{2}X_2 - \kappa X_1X_2 - X_8,$$

$$\dot{X}_9 = 3[X_7 - X_8]. \tag{47}$$

The nonlinear system [Eq. (47)] is the set of moment evolution equations for the Duffing nanoresonator. We reiterate that positive and negative values for η correspond to the hardening and softening Duffing potentials. We solve the moment evolution equations for various values of η in the sequel, noting that the linear case is obtained by setting $\eta=0$ in Eq. (47). Indeed, for this case the equations collapse to the closed moment system obtained in Ref. 23.

In order to understand the effects of varying η, we set $\kappa=0.1$ and $\epsilon=0.3$ in all our cases. The choice of these values for κ (which measures the interaction strength between the SET and the resonator) and ϵ (which compares the relative time scales of the resonator period and the electron-tunneling time) is guided by the fact that the model is only valid for both κ and ϵ much less than unity.[23] However, extremely weak coupling between the SET and the resonator (for instance, say, $\kappa=0.01$) could mask the uniquely nonlinear effects and hence our choice is influenced by this aspect as well. In this context, we would like to draw a distinction between the coupling strength of the SET-resonator interaction and the dynamical effects that arise due to nonlinear resonator motion. We emphasize this important point in discussing our results. We also note here that in all the cases, initial conditions on P_N and P_{N+1} are taken to be sharply peaked Gaussian densities with mean value of 0.5 and variance of 0.006 25.

V. DUFFING POTENTIAL WITH HARDENING STIFFNESS

In this section we consider the Duffing potential with hardening stiffness, numerically solving the moment evolu-

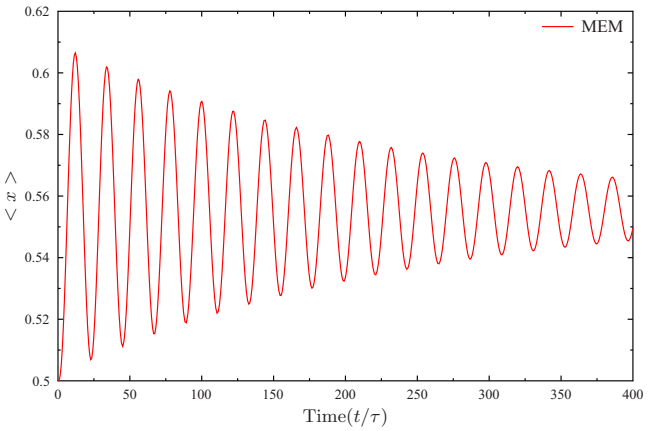

FIG. 2. (Color online) Mean displacement of the resonator: $\eta=0$.

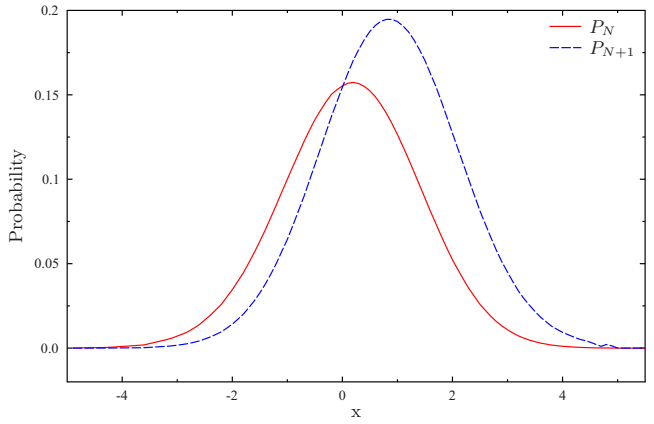

FIG. 3. (Color online) Steady state probability subdensities: $\eta=0$.

tion [Eq. (47)] for the cases $\eta=0.5$, $\eta=0.75$, and $\eta=1$. However, in order to compare our results with the linear case we first solve the latter case with $\eta=0$. The FEM solutions are utilized to validate the approximations invoked in obtaining moment closure in each of the nonvanishing η cases. Additionally, the steady-state probability densities are obtained from the FEM solutions in each of the cases.

A. Linear case

Setting $\eta=0$, the system of moment evolution [Eq. (47)] collapses to the following system of equations:

$$\dot{X}_1 = X_2,$$

$$\dot{X}_2 = -\epsilon^2[X_1 - X_3],$$

$$\dot{X}_3 = -X_3 + \frac{1}{2} + \kappa X_1. \tag{48}$$

Indeed, these are the moment evolution equations obtained in Ref. 23. The resonator response is presented in Fig. 2 and clearly, the resonator motion is damped by the SET and the system reaches a steady state. The steady-state-density functions are given in Fig. 3.

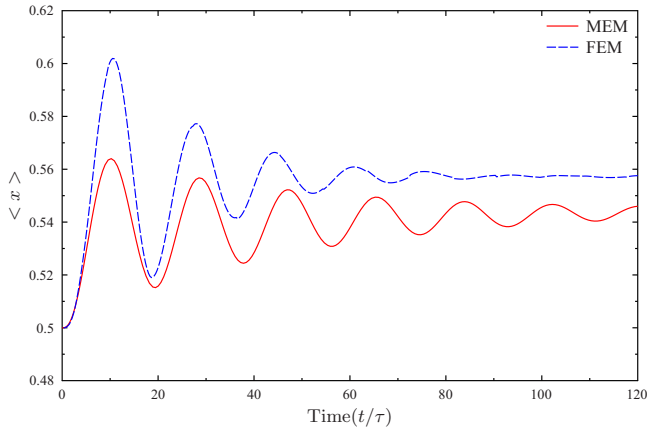

FIG. 4. (Color online) Mean displacement of the resonator: $\eta=0.5$.

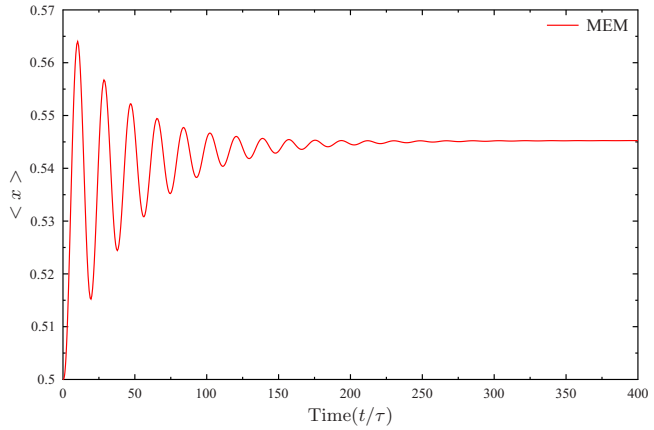

FIG. 5. (Color online) Mean displacement of the resonator: $\eta=0.5$.

B. Case $\eta=0.5$

1. Mean displacement

In Fig. 4 we present a comparison of the time evolution of the mean resonator displacement for the case $\eta=0.5$ obtained from the FEM and the MEM. First, we note that the mean resonator displacement is asymptotically stationary implying that the system attains a steady state. Keeping in mind that the solutions obtained from the two methods cannot be expected to agree entirely due to the approximations involved in the MEM, the second point is that the maximum difference in peak amplitudes (which occurs in the first period) is about 6%. Furthermore, the difference in the (scaled) mean displacement when the system is very close to the steady state at time $t/\tau=120$ is about 0.013. Therefore, we conclude that the two solutions are in good qualitative agreement and that the MEM solution is a good approximation to the resonator displacement in this case. In Fig. 5 we present the MEM solution for the resonator displacement plotted until $t/\tau=400$.

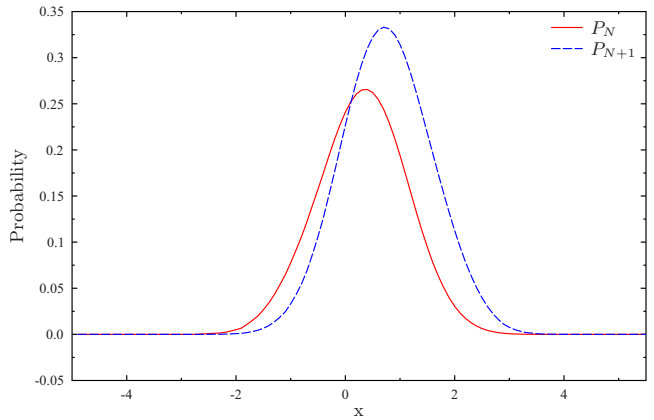

FIG. 6. (Color online) Steady state probability subdensities: $\eta=0.5$.

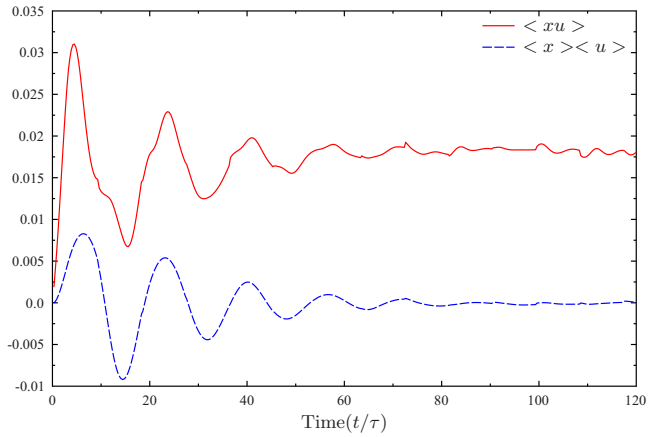

FIG. 7. (Color online) Comparison from FEM: η=0.5.

The damping of the resonator motion observed in Figs. 4 and 5 clearly indicates that the resonator reaches a steady state. The probability density functions P_N and P_{N+1} corresponding to the steady state are presented in Fig. 6.

2. Moment approximations

In order to further examine the validity of the moment approximations used in the MEM, we now plot the time evolution of each one of the approximations using the FEM solution. In other words, we know precisely the approximations that have been made in the MEM and we would like to examine their validity in the light of the FEM solution. We recall from Eq. (34) that the approximations used in deriving the moment evolution equations are given by

$$\langle x^2u\rangle \approx \langle x^2\rangle\langle u\rangle,$$

$$\langle ux\rangle_{N+1} \approx \langle u\rangle_{N+1}\langle x\rangle_{N+1},$$

$$\langle ux\rangle \approx \langle u\rangle\langle x\rangle,$$

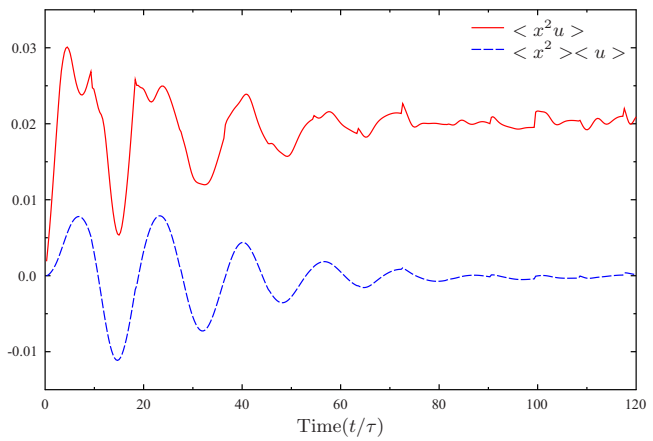

FIG. 8. (Color online) Comparison from FEM: η=0.5.

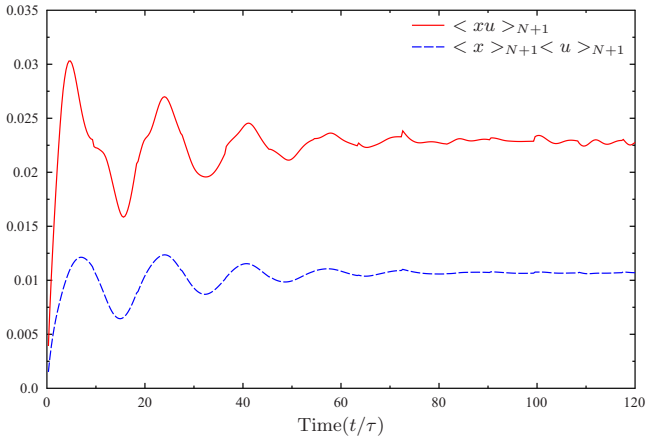

FIG. 9. (Color online) Comparison from FEM: η=0.5.

$$\langle x^2u\rangle_N \approx \langle x^2\rangle_N\langle u\rangle_N. \tag{49}$$

We present a comparison of the time evolution of each one of the above approximations as computed from the FEM solution in Figs. 7–10.

It is of interest to observe the qualitative similarity in Figs. 7–9 between the exact result (the moment of the products) and the approximation (the product of the moments). Furthermore, we observe from Figs. 7 and 8 that the approximations tend to zero at t/τ=120 while the exact values are nonzero. This is explained based on the fact that in each of these cases the approximation involves a product, a term in which is the mean resonator velocity $\langle u\rangle$. The mean resonator velocity tends to zero in the steady state and the products involved in the approximation vanish as well. The numerical difference between the exact and approximate values in Fig. 9 is 0.0125 at t/τ=120 while it is 0.0175 from Fig. 10. The main point of this exercise is to buttress the moment approximations by demonstrating that the approximations do not lead to significant divergences. Indeed, this ultimately reflects in the agreement between the FEM and MEM solutions observed in Fig. 4.

3. Variance

The time evolution of the variance of the displacement is presented in Fig. 11. It is observed that the variance settles

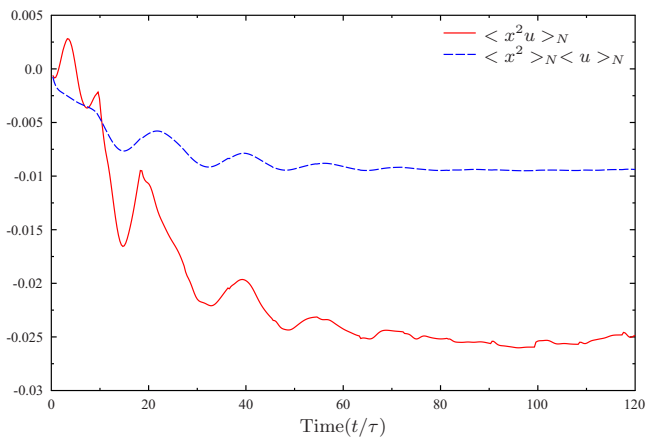

FIG. 10. (Color online) Comparison from FEM: η=0.5.

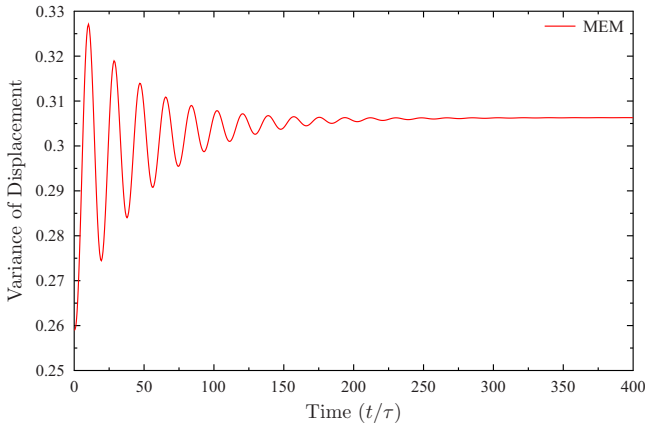

FIG. 11. (Color online) Evolution of variance of displacement: η=0.5.

down to a constant value of approximately 0.305 as the system approaches the steady state. This result, combined with the behavior of the mean displacement, is further confirmation that, indeed, the system reaches a steady state. The steady-state value of variance of the displacement has implications for the steady-state effective temperature attained by the system and hence the behavior of the variance of the displacement with respect to the strength of the nonlinearity is an important aspect of the analysis. We take up this point for discussion in our conclusions. In this nonlinear case of η=0.5, our analysis thus far has established that the MEM is a reasonable approximation and that the SET-resonator system attains a steady state. From comparing Figs. 2 and 5 we then draw the important conclusion that the SET damps the resonator at a significantly higher rate due to the nonlinearity in the resonator motion. As will be seen in the next cases corresponding to η=0.75 and η=1, this is a consistent result since the rate at which the SET damps the resonator increases with η, the strength of the nonlinearity in the resonator motion.

C. Case η=0.75

We now consider the case of a stronger nonlinearity given by η=0.75. The analysis proceeds along the lines of the η =0.5 case.

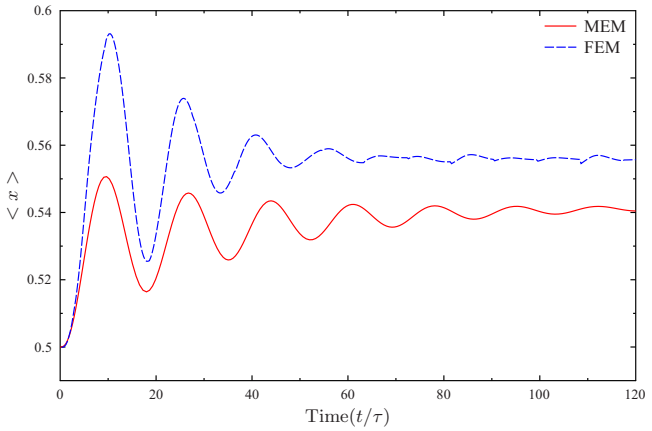

FIG. 12. (Color online) Mean displacement of the resonator: η =0.75.

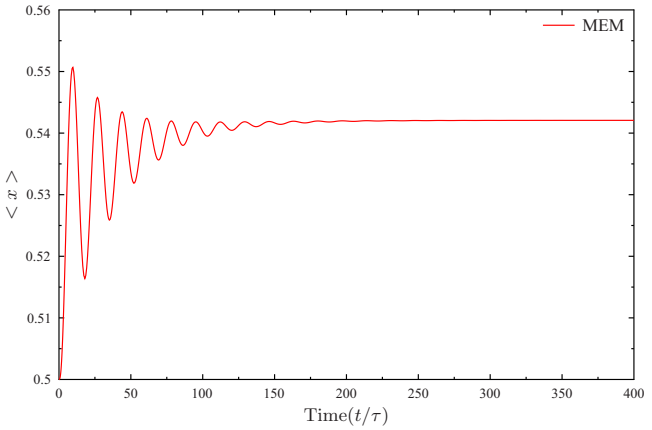

FIG. 13. (Color online) Mean displacement of the resonator: η =0.75.

1. Mean displacement

In Fig. 12 we present a comparison of the time evolution of the mean resonator displacement for the case η=0.75 obtained from the FEM and the MEM. The maximum difference in peak amplitudes (which again occurs in the first period) is about 7.5% in this case. The difference in the (scaled) mean displacement when the system begins to approach the steady state at time t/τ=120 is about 0.018. These values are slightly higher than those obtained in the η=0.5 case. This is to be expected since increasing the strength of the nonlinearity certainly implies more complicated dynamics. However, the two solutions are still in good qualitative agreement and hence the MEM solution continues to be a good approximation to the resonator displacement. In Fig. 13 we present the MEM solution for the resonator displacement plotted until t/τ=400. The probability density functions P_N and P_{N+1} corresponding to the steady state obtained from the FEM solution are presented in Fig. 14.

2. Moment approximations

Since the consistency of the moment approximations is not guaranteed when the strength of the nonlinearity is increased, we examine the approximations in closer detail in

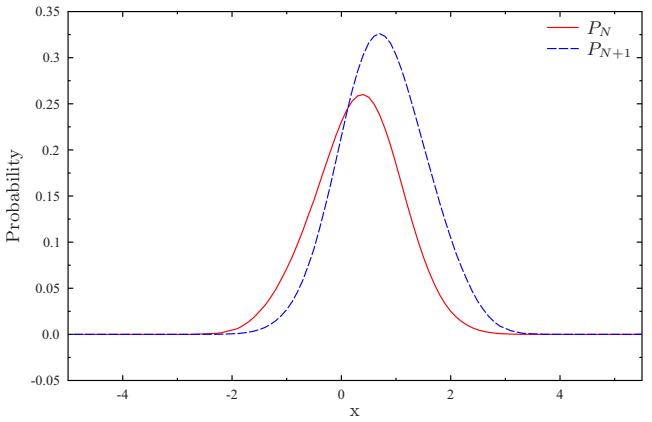

FIG. 14. (Color online) Steady state probability subdensities: η=0.75.

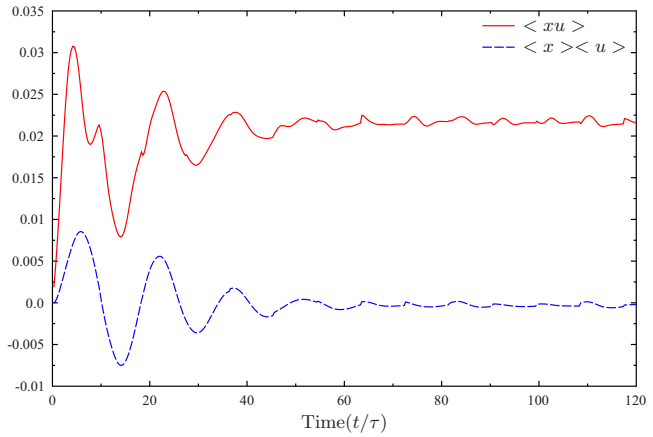

FIG. 15. (Color online) Comparison from FEM: η=0.75.

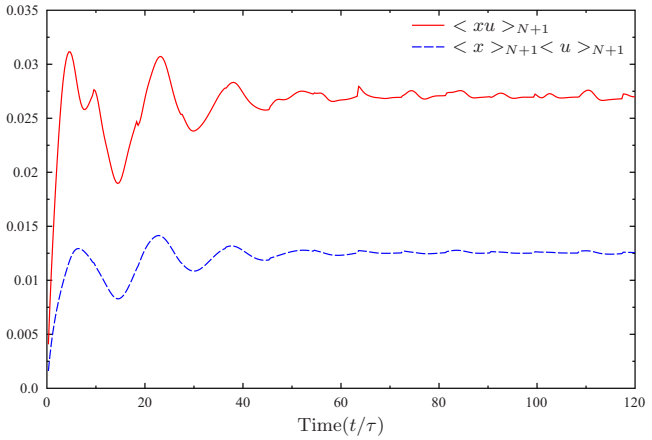

FIG. 17. (Color online) Comparison from FEM: η=0.75.

the present case as well. We present a comparison of the time evolution of each one of the moment approximations as computed from the FEM solution in Figs. 15–18.

We observe that the qualitative similarity in Figs. 15–17 between the exact result (the moment of the products) and the approximation (the product of the moments) implies that our conclusions from the previous case of η=0.5 continue to hold in this case as well. The disagreement between the exact and the approximate quantities is most severe in the case of the product $\langle x^2\rangle_N\langle u\rangle_N$ (Fig. 18). There exists even a qualitative difference between the moment of the product and the product of the moments as the former increases initially before showing a significant drop at around t/τ=5 whereas the latter decreases monotonically with respect to (scaled) time. However, asymptotically both the exact and approximate quantities tend to constant values. Overall, even though the difference between the exact and approximate values in the steady state shows an increase (Figs. 15–18) when compared to the η=0.5 case, the behavior is still not significantly different as to challenge the validity of the approximations.

3. Variance

The time evolution of the variance of the displacement is presented in Fig. 19. It is observed that the variance settles down to a constant value of approximately 0.302 as the system approaches the steady state. This result, combined with the behavior of the mean displacement, is further confirmation that, indeed, the system reaches a steady state. Furthermore, it is important to note here that the steady-state variance has attained a lower value in this case when compared to the case of η=0.5. When we compare Fig. 13 with Figs. 2 and 5 it is clear that the rate at which the SET damps the resonator motion increases with increasing η. As a final case in our analysis we consider η=1 in Sec. V D.

D. Case η=1

We now present the strongest nonlinear case that we consider given by η=1.0. The analysis is very similar to that carried out for the previous cases. In Fig. 20 we present a comparison of the time evolution of the mean resonator displacement for the case η=1.0 obtained from the FEM and the MEM. The maximum difference in peak amplitudes (which again occurs in the first period) is about 9.2% in this case. The difference in the (scaled) mean displacement when the system begins to approach the steady state at time t/τ =120 is about 0.019. As is to be expected, these values are slightly higher than those obtained in the previous cases. However, the two solutions continue to be in good qualitative agreement and hence the MEM solution continues to be

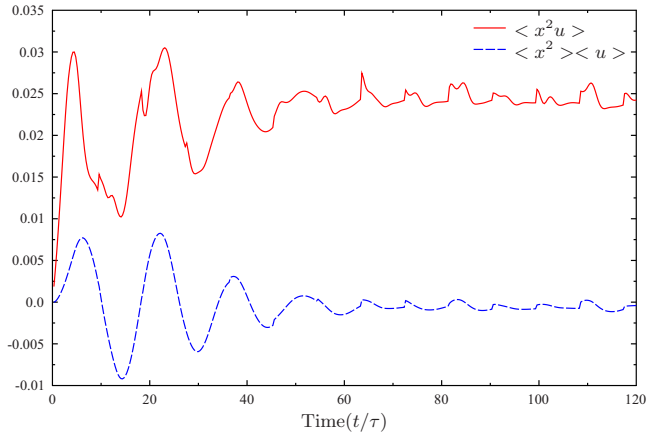

FIG. 16. (Color online) Comparison from FEM: η=0.75.

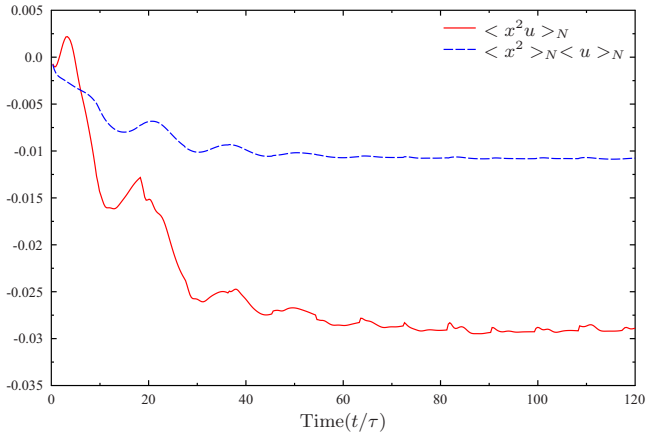

FIG. 18. (Color online) Comparison from FEM: η=0.75.

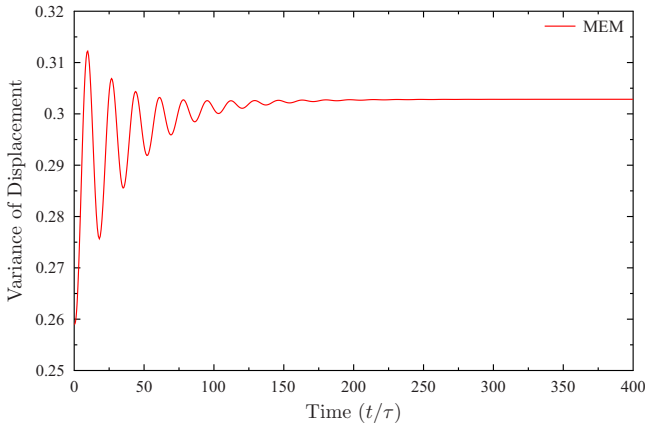

FIG. 19. (Color online) Evolution of variance of displacement: η=0.75.

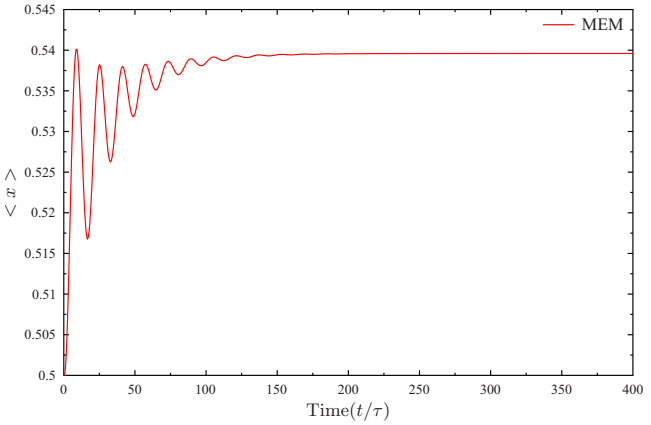

FIG. 21. (Color online) Mean displacement of the resonator: η =1.

a good approximation to the resonator displacement. In Fig. 21 we present the MEM solution for the resonator displacement plotted until t/τ=400. The probability subdensity functions P_N and P_{N+1} corresponding to the steady state obtained from the FEM solution are presented in Fig. 22.

1. Moment approximations

As in the previous cases, we present a comparison of the time evolution of each one of the moment approximations as computed from the FEM solution in Figs. 23–26. The behavior of the moments in Figs. 23–26 confirms that the approximations continue to hold in the qualitative sense. However, quantitatively the difference between the steady-state values of the exact and approximate quantities has increased compared to all the previous cases. Therefore the approximation, while still valid, becomes increasingly divergent from the exact value as the strength of the nonlinearity is increased.

2. Variance

The time evolution of the variance of the displacement is presented in Fig. 27. It is observed that the variance settles down to a constant value of approximately 0.3 as the system approaches the steady state. This interesting result is consistent with the previous cases and clearly indicates that the steady-state variance of the resonator displacement keeps decreasing as the strength of the nonlinearity is increased. Now on comparing Figs. 2, 5, 13, and 22 we conclude that the SET damps the resonator most effectively for η=1. We also mention a point here that is taken up for further discussion in Sec. VI A. In the linear case (Fig. 2), the steady-state value of the displacement is precisely the mean value during the first period. As the strength of the nonlinearity is increased, the steady-state mean values tend to increase as seen from Figs. 5, 13, and 21. Therefore, apart from the conclusion that the resonator approaches the steady state more rapidly for higher values of η, we also observe that the damping mechanism undergoes qualitative changes as the strength of the nonlinearity is increased. The results obtained in this section are taken up for a detailed discussion in Sec. VII of the paper.

VI. DUFFING POTENTIAL WITH SOFTENING STIFFNESS

In this section we consider solutions of Eq. (47) for cases with negative values of η. In comparison with the results

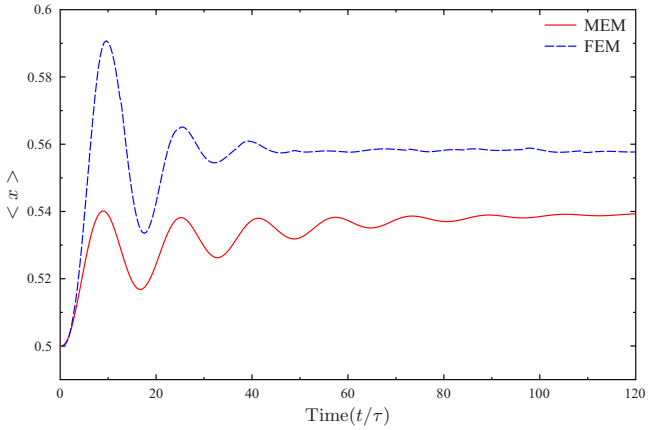

FIG. 20. (Color online) Mean displacement of the resonator: η =1.

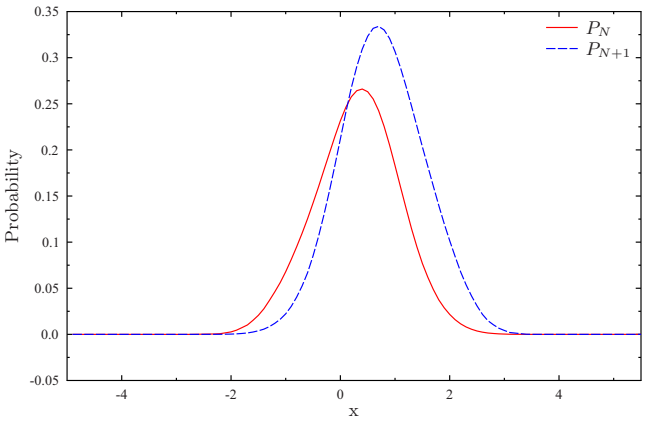

FIG. 22. (Color online) Steady state probability subdensities: η=1.

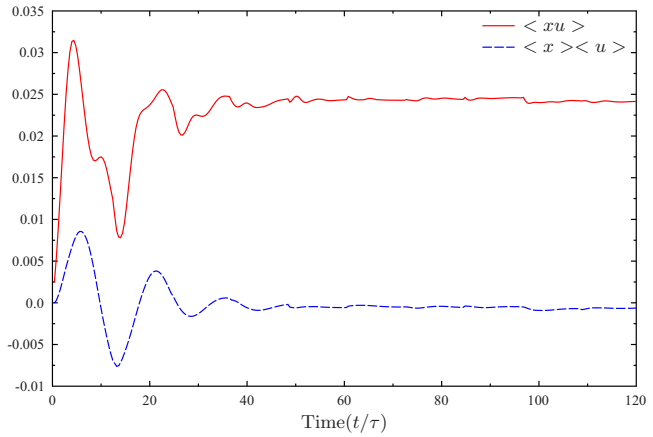

FIG. 23. (Color online) Comparison from FEM: η=1.

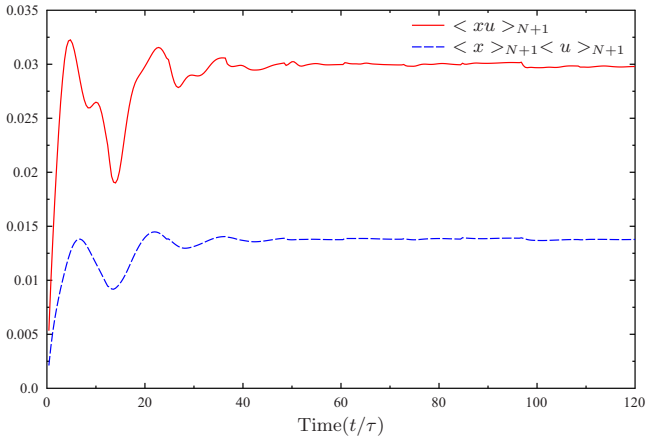

FIG. 25. (Color online) Comparison from FEM: η=1.

obtained in Sec. V D 2, the dynamics are qualitatively different in this case. We note here that the values of η, chosen based on an extensive numerical investigation, are intended to depict the interesting qualitative changes in the dynamics.

A. Case η=−0.04

We solve the system of moment equations for η=−0.04 and in Fig. 28 present a comparison of the mean displacement of the resonator with the linear case. It is seen that it takes more time for the system to reach a steady state in the case of η=−0.04. In other words, the SET damps the resonator motion much more effectively in the linear case than in the presence of the softening stiffness Duffing nonlinearity. As will be evident from the cases that follow, this is a precursor to the dramatic changes in the resonator dynamics triggered by variations in η in the softening Duffing case. Moreover, we note here the contrast with the hardening Duffing case where the presence of nonlinearity enhances the damping effect thereby forcing the system to the steady state more rapidly.

We present the phase portrait in Fig. 29. From the figure it is evident that the system approaches the equilibrium point described by the coordinates (0.56,0.0) in the phase plane and that the equilibrium point is a focus.

B. Case η=−0.09

In order to investigate further the reticence of the SET in damping the resonator motion, we now increase the magnitude (absolute value) of the nonlinearity to η=−0.09. The result is presented in Fig. 30. Evidently, the SET is increasingly ineffective in damping the resonator motion as the magnitude of η is increased.

C. Case η=−0.11

We now present the most interesting case of η=−0.11. The mean resonator displacement versus time is presented in Fig. 31. As seen from the figure, the resonator motion is totally undamped in this case. In other words, no energy transfer occurs between the SET and the resonator and the coupled system is in a state of dynamic equilibrium with the resonator exhibiting self-sustained oscillations. The implications of this important result are taken up for discussion in Sec. VI D. The presence of self-sustained oscillations in a nonlinear dynamical system is strongly indicative of a periodic attractor and indeed we find one as seen from Fig. 32. We note here that the existence of such periodic attractors is a unique feature of nonlinear systems. Furthermore, it is noteworthy that while limit cycles are well understood in the context of deterministic systems, the cycle in our case has

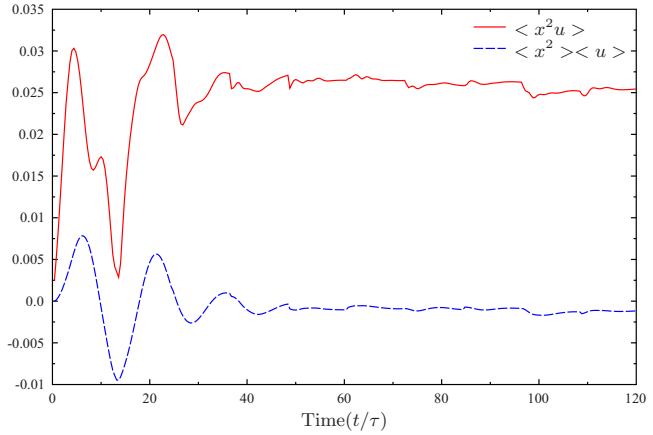

FIG. 24. (Color online) Comparison from FEM: η=1.

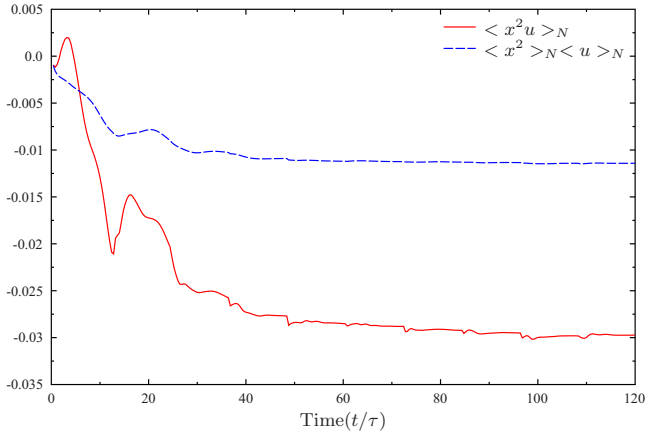

FIG. 26. (Color online) Comparison from FEM: η=1.

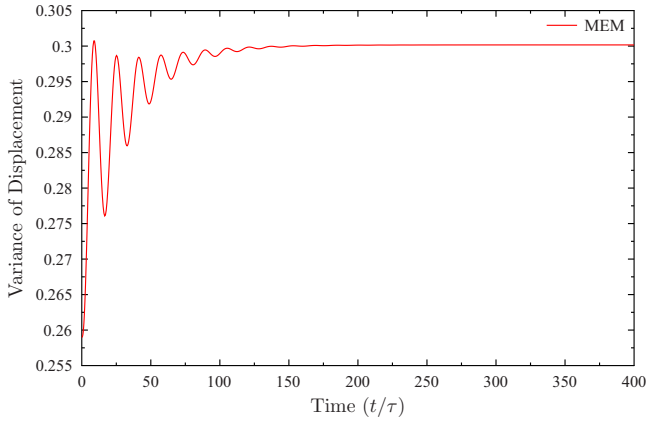

FIG. 27. (Color online) Evolution of variance of displacement: η=1.0.

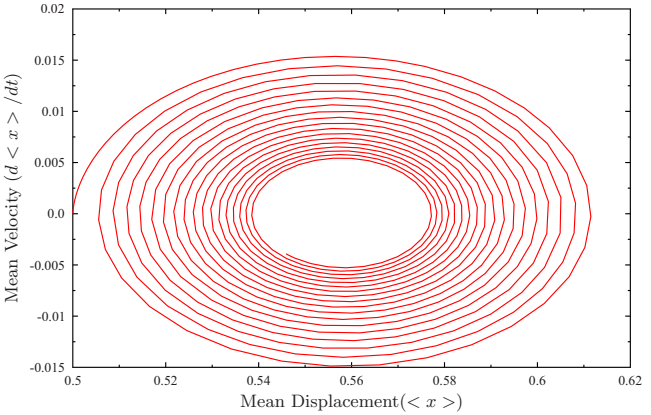

FIG. 29. (Color online) Phase portrait: η=−0.04.

emerged in the averaged dynamics of a stochastic system.

D. Case η=−0.25

Given the existence of a periodic solution for η=−0.11, it is natural to ask the question of what happens when the modulus of η is increased further. Here we present the results for the case η=−0.25. The mean resonator displacement versus time is presented in Fig. 33 and the phase portrait is given in Fig. 34. Remarkably, we observe the emergence of instability in this case. From Fig. 33 we see that the resonator exhibits oscillation, the magnitude of which grows unboundedly. This is corroborated by the phase portrait in Fig. 34 which indicates an unstable focus. Physically, this corresponds to the situation that the SET continuously supplies energy to the oscillator.

Our results in this section clearly point to the fact that the dynamics of the SET-resonator system is uniquely sensitive to the strength of the nonlinearity in softening stiffness Duffing case. Early evidence of the inability of the SET to damp the resonator motion was observed in Fig. 28 from which we concluded that even when compared to the case of a weakly nonlinear softening Duffing potential, the system reaches the steady state much faster in the presence of a linear harmonic potential. The ability of the SET to effectively damp the resonator motion deteriorated further, with an increase in the magnitude of the strength of the nonlinearity. Finally, at η =−0.11 we observed that the resonator had attained a dynamical state of equilibrium with the SET and there was no energy transfer in either direction. When the magnitude of the strength of the nonlinearity was increased further, we witnessed a dynamical instability at η=−0.25. Indeed the instability sets in for any value of η less than −0.11 but we choose to demonstrate it at η=−0.25 for enhanced clarity of the results. These results are discussed further in Sec. VII.

VII. DISCUSSION AND CONCLUSIONS

Our conclusions from the analysis of the SET-resonator system in the Duffing regime naturally fall under two cases: the hardening stiffness case and the softening stiffness case. In the hardening stiffness case, the primary observation is that the system indeed reaches a steady state as in the case of the linear resonator. We note that this is far from obvious *a priori* since there is no guarantee that the SET would damp the resonator motion in the nonlinear regime. Significantly, the rate of damping is much higher in the nonlinear case.

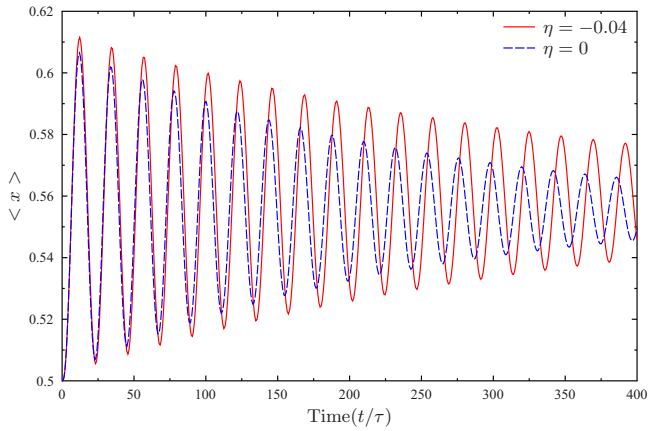

FIG. 28. (Color online) Comparison of mean displacement of the resonator.

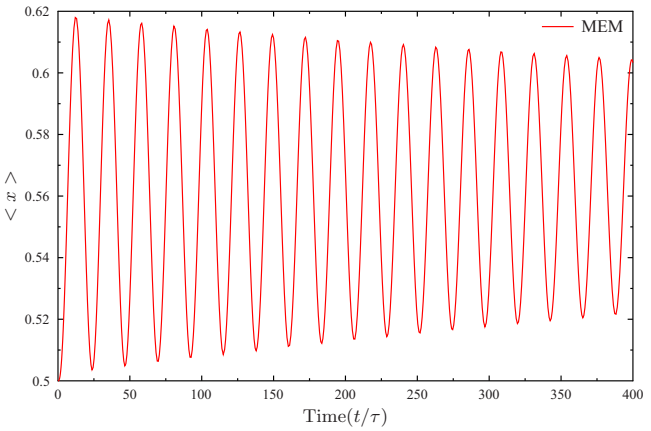

FIG. 30. (Color online) Mean displacement of the resonator: η =−0.09.

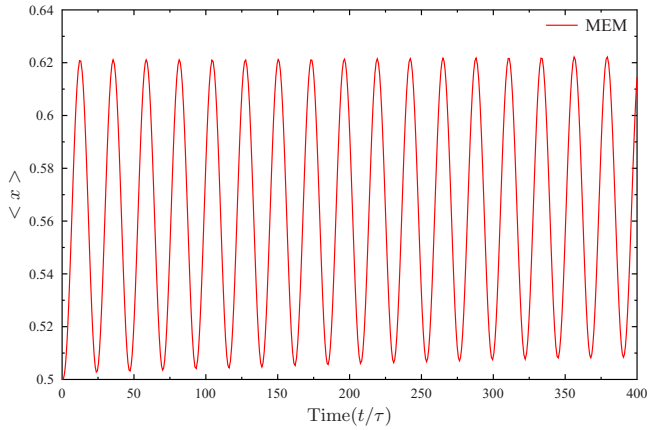

FIG. 31. (Color online) Mean displacement of the resonator: $\eta = -0.11$.

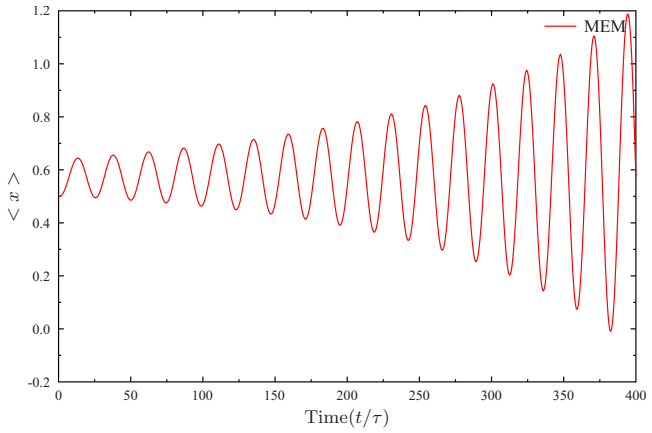

FIG. 33. (Color online) Mean displacement of the resonator: $\eta = -0.25$.

Furthermore, the rate of damping markedly increases with the effective nonlinearity in the system (represented by the parameter η). It is also to be noted here that the increased efficacy of the SET in damping the nonlinear resonator motion is further evidenced by the fact that the mean amplitude of the first period of oscillation of the resonator decreases with increasing η. Whereas we observe a value of approximately 0.605 (Fig. 2) for the first period of resonator oscillation in the linear case, this reduces to approximately 0.54 (Fig. 21) when $\eta=1$. It is important to note here that the higher rate of damping arises exclusively due to the SET-resonator interaction since we have not considered any extrinsic source of damping in our model. The next point is that our results are obtained for relatively weak coupling between the SET and the resonator ($\kappa=0.1$), which is the most readily accessible regime in current experiments. Hence we conclude that nonlinearity in the resonator motion significantly impacts the dynamics of the coupled system even for weak coupling between the SET and the resonator. This is noteworthy since often nonlinear effects are associated with strongly coupled systems.

It is interesting to consider the implications of our results for SET sensitivity from a practical viewpoint. The SET can be effectively used as a displacement detector for the nanoresonator only after the steady state is achieved for the coupled dynamics. The conclusion that this steady state is achieved more rapidly in the nonlinear case seems to indicate that the coupled system would work better as a sensor in the nonlinear regime.

An important aspect of the system studied in this paper is the effective temperature attained by the system in the steady state. Lower steady-state effective temperatures are highly desirable for classical measurements while they are critical in quantum coherent measurements.[19] We note here that the classical theorem of equipartition of energy may be extended to nonlinear Hamiltonian systems[37] in order to define a steady-state effective temperature. While in a parallel effort we utilize this idea explicitly in a Fokker-Planck approach to the SET-resonator system in the Duffing regime,[38] it is interesting to note here from Figs. 11, 19, and 27 that the steady-state value of the variance of the displacement attained by the oscillator decreases with increasing η. The difference in numerical values is not large as seen from the figures but it exists. Since in the steady state the variance of the displacement is directly proportional to the absolute temperature of the oscillator, we conclude that nonvanishing η, in fact, pushes the oscillator to a steady state of lower temperature as compared to the linear case. Thus, our analysis indicates that, in fact, better cooling of the resonator is achieved in the hardening stiffness Duffing regime.

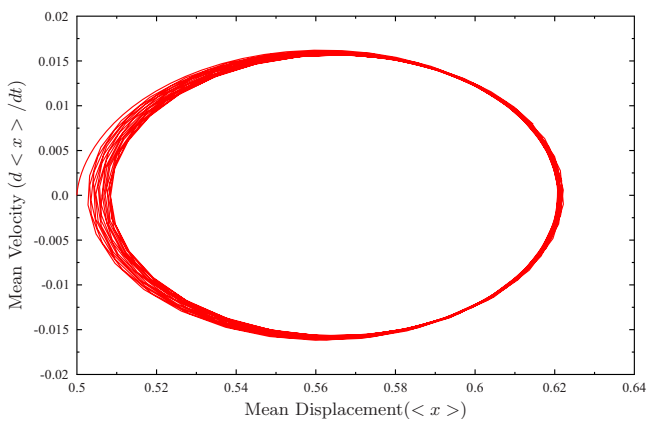

FIG. 32. (Color online) Phase portrait: $\eta = -0.11$.

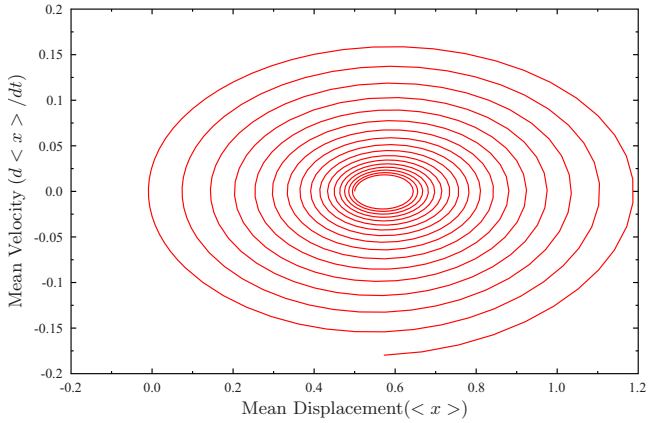

FIG. 34. (Color online) Phase portrait: $\eta = -0.25$.

Finally, we observe from Figs. 5, 13, and 22 that the steady-state mean value of the resonator displacement tends to increase with the strength of the nonlinearity. This points to a qualitative change in the damping mechanism in the strongly nonlinear regime. We believe this to be an important observation unique to the nonlinear regime characterized by the hardening stiffness Duffing potential.

In the softening stiffness Duffing case in the presence of very weak nonlinearity the SET damps the resonator and the coupled system reaches a steady state. However, in the presence of the double-well Duffing potential the SET finds it harder to damp the resonator motion than in the linear case. Moreover, the inability of the SET to damp the resonator becomes acute as the strength of the nonlinearity is increased. For the parameter values that we have consistently adhered to in this paper ($\epsilon=0.3$ and $\kappa=0.1$), we observed that for a critical value of $\eta=-0.11$, the SET, and the resonator reach a state of dynamical equilibrium characterized by the presence of a periodic orbit in the phase space. Indeed, in comparison with the linear harmonic and the hardening stiffness Duffing potentials, this phenomenon is unique to the softening stiffness Duffing regime emphasizing that the sign of η critically influences the dynamics.

Finally, we observe the onset of instability below the critical value of $\eta=-0.11$. Again, such a clear onset of instability is observed only in the double-well Duffing regime. There has been a lot of recent interest in the phenomenon of the SET pumping energy into the resonator in specific dynamical regimes known as back action (see, for instance, Refs. 19 and 25). While most of the discussion in the literature is focused on back action as a consequence of unique processes in the SET, our analysis points to a specific situation where this can emerge as a purely nonlinear effect—the onset of a dynamical instability in the SET-resonator system. In the broad context of nonlinear dynamics of NEMS, knowledge of the existence of such instabilities can be expected to aid the design and operation of these systems.

In summary, our analysis of the Duffing regime of a nanomechanical resonator coupled to a SET leads to a set of interesting conclusions in the case of the currently experimentally relevant regime of weak coupling between the device and the resonator. We hope that our results motivate efforts to obtain their experimental validation.

ACKNOWLEDGMENTS

We would like to especially thank Bala Sundaram, Miles Blencowe, Andrew Armour, and Keith Schwab for useful discussions. One of us (S.R.) would like to gratefully acknowledge financial support from the School of Engineering, Rutgers University during the time this work was undertaken.

*benaroya@rci.rutgers.edu

[1] M. L. Roukes, Sci. Am. **285**, 48 (2001).
[2] M. L. Roukes, Phys. World **14**, 25 (2001).
[3] H. G. Craighead, Science **290**, 1532 (2000).
[4] A. N. Cleland, *Foundations of Nanomechanics* (Springer, Heidelberg, 2002).
[5] R. H. Blick, A. Erbe, L. Pescini, A. Kraus, D. V. Scheible, F. W. Beil, E. Hoehberger, A. Hoerner, J. Kirschbaum, H. Lorenz, and J. P. Kotthaus, J. Phys.: Condens. Matter **14**, R905 (2002).
[6] M. P. Blencowe, Phys. Rep. **395**, 159 (2004).
[7] M. P. Blencowe, Contemp. Phys. **46**, 249 (2005).
[8] M. P. Blencowe and M. N. Wybourne, Appl. Phys. Lett. **77**, 3845 (2000).
[9] Y. Zhang and M. P. Blencowe, J. Appl. Phys. **91**, 4249 (2002).
[10] R. G. Knobel and A. N. Cleland, Nature (London) **424**, 291 (2003).
[11] M. D. LaHaye, O. Buu, B. Camarota, and K. C. Schwab, Science **304**, 74 (2004).
[12] X. M. Henry Huang, C. A. Zorman, M. Mehregany, and M. L. Roukes, Nature (London) **421**, 496 (2003).
[13] K. L. Ekinci, X. M. H. Huang, and M. L. Roukes, Appl. Phys. Lett. **84**, 4469 (2004).
[14] K. L. Ekinci, Y. T. Yang, and M. L. Roukes, J. Appl. Phys. **95**, 2682 (2004).
[15] A. N. Cleland and M. L. Roukes, Nature (London) **392**, 160 (1998).
[16] J. A. Sidles, J. L. Garbini, K. J. Bruland, D. Rugar, O. Zuger, S. Hoen, and C. S. Yannoni, Rev. Mod. Phys. **67**, 249 (1995).
[17] A. Cho, Science **299**, 36 (2003).
[18] M. P. Blencowe, Science **304**, 56 (2004).
[19] A. Naik, O. Buu, M. D. LaHaye, A. D. Armour, A. A. Clerk, M. P. Blencowe, and K. C. Schwab, Nature (London) **443**, 193 (2006).
[20] A. Hopkins, K. Jacobs, S. Habib, and K. Schwab, Phys. Rev. B **68**, 235328 (2003).
[21] A. N. Cleland and M. R. Geller, Phys. Rev. Lett. **93**, 070501 (2004).
[22] D. K. Ferry and S. M. Goodnick, *Transport in Nanostructures* (Cambridge University Press, Cambridge, 1997).
[23] A. D. Armour, M. P. Blencowe, and Y. Zhang, Phys. Rev. B **69**, 125313 (2004).
[24] M. P. Blencowe, J. Imbers, and A. D. Armour, New J. Phys. **7**, 236 (2005).
[25] A. A. Clerk and S. Bennett, New J. Phys. **7**, 238 (2005).
[26] A. A. Clerk, Phys. Rev. B **70**, 245306 (2004).
[27] A. Erbe, H. Krommer, A. Kraus, R. H. Blick, G. Corso, and K. Richter, Appl. Phys. Lett. **77**, 3102 (2000).
[28] J. S. Aldridge and A. N. Cleland, Phys. Rev. Lett. **94**, 156403 (2005).
[29] R. Almog, S. Zaitsev, O. Shtempluck, and E. Buks, Appl. Phys. Lett. **90**, 013508 (2007).
[30] E. Buks and M. L. Roukes, J. Microelectromech. Syst. **11**, 802 (2002).
[31] R. L. Badzey and P. Mohanty, Nature (London) **437**, 995 (2005).
[32] D. V. Scheible, A. Erbe, R. H. Blick, and G. Corso, Appl. Phys. Lett. **81**, 1884 (2002).
[33] V. Peano and M. Thorwart, Phys. Rev. B **70**, 235401 (2004).
[34] C. B. Doiron, W. Belzig, and C. Bruder, Phys. Rev. B **74**,

205336 (2006).
[35] J. Guckenheimer and P. Holmes, *Nonlinear Oscillations, Dynamical Systems, and Bifurcations of Vector Fields* (Springer-Verlag, New York, 1983).
[36] M. Amman, R. Wilkins, E. Ben-Jacob, P. D. Maker, and R. C. Jaklevic, Phys. Rev. B **43**, 1146 (1991).
[37] R. C. Tolman, *The Principles of Statistical Mechanics* (Dover, New York, 1979), reprint of the 1938 original.
[38] S. Ramakrishnan, Y. Gulak, and H. Benaroya (unpublished).